Temperature dependent characterization of terahertz vibrations of explosives and related threat materials

Joseph S. Melinger,[1,*] S. Sree Harsha,[2] N. Laman,[2] and D. Grischkowsky[2]

[1]*Naval Research Laboratory, Electronics Science and Technology Division, Code 6812, Washington, D.C. 20375, USA*

[2]*School of Electrical and Computer Engineering, Oklahoma State University, Stillwater, Oklahoma 74078, USA*

**joseph.melinger@nrl.navy.mil*

Abstract: Waveguide terahertz time-domain spectroscopy (THz-TDS) is used to characterize the temperature dependent vibrational properties of three threat-related materials: 4-amino-dinitrotoluene (4A-DNT), pentaerythritol tetranitrate (PETN), and octahydro-1,3,5,7-tetranitro-1,3,5,7-tetrazocine (HMX). These materials are characterized as thin polycrystalline layers deposited in the 50 micron gap of a metal parallel plate waveguide. For each material waveguide THz-TDS at least partially resolves the underlying vibrational spectrum and reveals new features that have not been observed in previous free space measurements of these materials. Strong experimental evidence for a phase transformation is observed for 4A-DNT as the polycrystalline layer on the waveguide surface is cooled to near 200 K. For PETN a highly resolved spectrum containing eleven vibrational lines is observed at 11 K with full-width at half maximum linewidths ranging from 7 GHz to 40 GHz. Based on comparison to measurements in the literature, our PETN measurement suggests that it is possible to produce narrow linewidths from a polycrystalline layer that approach those from a single crystal. Finally, for HMX, a highly resolved vibrational spectrum is measured that is assigned to the metastable gamma polymorph.

OCIS codes: (300.6495) Spectroscopy, terahertz; (130.2790) Guided waves.

References and links

1. M. C. Kemp, P. F. Taday, B. E. Cole, J. A. Cluff, A. J. Fitzgerald, and W. R. Tribe, "Security applications of terahertz technology," Proc. SPIE-Int. Soc. Opt. Eng., **5070**, 44–52 (2003).
2. J. F. Federici, B. Schulkin, F. Huang, D. Gary, R. Barat, F. Oliveira, and D. Zimdars, "THz imaging and sensing for security applications: Explosives, weapons, and drugs," Semicond. Sci. Technol. **20**(7), S266–S280 2005).
3. W. H. Fan, A. Burnett, P. C. Upadhya, J. Cunningham, E. H. Linfield, and A. G. Davies, "Far-infrared spectroscopic characterization of explosives for security applications using broadband terahertz time-domain spectroscopy," Appl. Spectrosc. **61**(6), 638–643 (2007).
4. J. Barber, D. E. Hooks, D. J. Funk, R. D. Averitt, A. J. Taylor, and D. Babikov, "Temperature-dependent far-infrared spectra of single crystals of high explosives using terahertz time-domain spectroscopy," J. Phys. Chem. A **109**(15), 3501–3505 (2005).
5. N. Laman, S. Sree Harsha, D. Grischkowsky, and J. S. Melinger, "7 GHz resolution waveguide THz spectroscopy of explosives related solids showing new features," Opt. Express **16**(6), 4094–4105 (2008).
6. J. S. Melinger, N. Laman, and D. Grischkowsky, "The underlying terahertz spectrum of explosive solids," Appl. Phys. Lett. **93**, 011102 (2008).
7. T. Lo, I. S. Gregory, C. Baker, P. F. Taday, W. R. Tribe, and M. C. Kemp, "The very far-infrared spectra of energetic materials and possible confusion materials using terahertz pulsed spectroscopy," Vib. Spectrosc. **42**(2), 243–248 (2006).
8. J. Chen, Y. Chen, H. Zhao, G. J. Bastiaans, and X.-C. Zhang, "Absorption coefficients of selected explosives and related compounds in the range of 0.1-2.8 THz," Opt. Express **15**(19), 12060–12067 (2007).
9. Y. Hu, P. Huang, L. Guo, X. Wang, and C. Zhang, "Terahertz spectroscopic investigations of explosives," Phys. Lett. A **359**(6), 728–732 (2006).
10. M. R. Leahy-Hoppa, M. J. Fitch, X. Zheng, L. M. Hayden, and R. Osiander, "Wideband terahertz spectroscopy of explosives," Chem. Phys. Lett. **434**(4-6), 227–230 (2007).

#135522 - $15.00 USD Received 22 Sep 2010; revised 28 Oct 2010; accepted 2 Nov 2010; published 10 Dec 2010

11. J. Wilkinson, C. T. Konek, J. S. Moran, E. M. Witko, and T. M. Korter, "Terahertz absorption spectrum of triacetone triperoxide (TATP)," Chem. Phys. Lett. **478**(4-6), 172–174 (2009).
12. D. Allis, J. A. Zeitler, P. F. Taday, and T. A. Korter, "Theoretical analysis of the solid-state terahertz spectrum the high explosive RDX," Chem. Phys. Lett. **463**(1-3), 84–89 (2008).
13. D. G. Allis, and T. M. Korter, "Theoretical analysis of the terahertz spectrum of the high explosive PETN," ChemPhysChem **7**(11), 2398–2408 (2006).
14. J. Zhang, and D. Grischkowsky, "Waveguide terahertz time-domain spectroscopy of nanometer water layers," Opt. Lett. **29**(14), 1617–1619 (2004).
15. J. S. Melinger, N. Laman, and D. Grischkowsky, "The underlying terahertz vibrational spectrum of explosive solids'," Appl. Phys. Lett. **93**, 011102 (2008).
16. M. van Exter, and D. Grischkowsky, "Characterization of an optoelectronic terahertz beam system," IEEE Trans. Microw. Theory Tech. **38**(11), 1684–1691 (1990).
17. J. S. Melinger, N. Laman, S. S. Harsha, S. F. Cheng, and D. Grischkowsky, "High-resolution waveguide terahertz spectroscopy of partially oriented organic polycrystalline films," J. Phys. Chem. A **111**(43), 10977–10987 (2007).
18. J. S. Melinger, S S. Harsha, N. Laman, and D. Grischkowsky, "Guided-wave terahertz spectroscopy of molecular solids," J. Opt. Soc. Am. B **26**, A79–A89 (2009).
19. D. Graham, A. R. Kennedy, C. J. McHugh, W. E. Smith, W. I. F. David, K. Shankland, and N. Shankland, "The crystal structures of three primary products from the selective reduction of 2,4,6,-trinitrotoluene," N. J. Chem. **28**(1), 161–165 (2004).
20. F. Demartin, G. Filippini, A. Gavezzotti, and S. Rizzato, "X-ray diffraction and packing analysis on vintage crystals: Wilhelm Koerner's nitrobenzene derivatives from the School of Agricultural Sciences in Milano," Acta Crystallogr. B **60**(Pt 5), 609–620 (2004).
21. H. Cady, and A. C. Larson, "Pentaerythritol tetranitrate II: its crystal structure and transformation to PETN I; an algorithm for refinement of crystal structures with poor data," Acta Crystallogr. B **31**(7), 1864–1869 (1975).
22. C. T. Konek, B. P. Mason, J. P. Hooper, C. A. Stoltz, and J. Wilkinson, "Terahertz absorption spectra of 1,3,5,7-tetranitro-1,3,5,7-tetrazocane (HMX) polymorphs," Chem. Phys. Lett. **489**(1-3), 48–53 (2010).
23. P. Main, R. E. Cobbledick, and R. W. H. Small, "Structure of the fourth form of 1,3,5,7-tetra azacyclooctane (γ-GNX),2C4H8N8O8.0.5H2O," Acta Crystallogr. C **41**, 1351-1354 (1985).
24. H. Cady, A. C. Larson, and D. T. Cromer, "The crystal structure of α-HMX and a refinement of the structure of β-HMX," Acta Crystallogr. **16**(7), 617–623 (1963).
25. R. E. Cobbledick, and R. W. H. Small, "The crystal structure of the δ-form of 1,35,7-tetranitro-1,3,5,7 tetraazocyclooctane (δ-HMX)," Acta Crystallogr. B **30**(8), 1918–1922 (1974).
26. D. G. Allis, D. A. Prokhorova, and T. M. Korter, "Solid-state modeling of the terahertz spectrum of the high explosive HMX," J. Phys. Chem. A **110**(5), 1951–1959 (2006).
27. K.C. Oppenheim, T.M. Korter, J.S. Melinger, and D. Grischkowsky, "A solid-state density functional theory investigation of the structural isomers 1,2-dicyanobenzene and 1,3-dicyanobenzene" accepted for publication in J. Phys. Chem. A.

1. Introduction

Terahertz (THz) spectroscopy (0.1 THz – 10 THz; 0.3 cm^{-1} – 333 cm^{-1}) has become an important tool for studying the low frequency vibrational properties of molecules in the condensed phase. In addition to fundamental studies, THz spectroscopy has also shown strong potential for defense and security applications related to the detection of threat materials [1,2]. The ability to use THz spectroscopy for this application will be enhanced by obtaining a deeper fundamental understanding of THz vibrational spectra.

Recent experimental [3–11] and theoretical [12,13] studies have shown that explosive molecules (and related threat molecules) in the crystalline environment exhibit complex vibrational structure in the THz region. The complexity may be understood by considering the vibrations of a unit cell that contains Z molecules and N atoms, leading to a prediction of 3N–6Z intramolecular vibrations and 6Z–3 intermolecular vibrations (phonons). The intramolecular vibrations in the THz region tend to involve the motion of all the atoms in the molecule, and therefore they can be very sensitive to the surroundings. In the crystalline environment the intramolecular and intermolecular modes can interact, resulting in vibrational modes with mixed intramolecular and intermolecular character [12,13]. From these considerations the THz vibrational spectrum of an explosive solid is predicted to contain a highly detailed fingerprint.

To date, there have been several investigations of the far infrared properties of explosives solids and their related derivatives and simulation materials [3–11]. These studies have shown that many of the explosive solids have distinct vibrational absorption features at room temperature that can be used for characterization and identification. These absorption features

#135522 - $15.00 USD Received 22 Sep 2010; revised 28 Oct 2010; accepted 2 Nov 2010; published 10 Dec 2010

tend to be rather broad and overlapping with Q factors ($f/\Delta f$) typically < 10. The broad absorption features are a consequence of the broadening of the underlying individual THz resonances due to homogeneous and inhomogeneous line broadening mechanisms. The resolution of the underlying THz resonances of an explosives solid is a challenging problem and is necessary to achieve a full understanding of the THz properties of explosives, and to make rational use of database THz spectra for detection applications.

In this paper we use waveguide terahertz time domain spectroscopy (THz-TDS) to study the temperature dependence of the THz vibrational spectra for the explosives-related solid 4-amino-dinitrotoluene (4A-DNT), and the explosives solids pentaerythritol tetranitrate (PETN) and octahydro-1,3,5,7-tetranitro-1,3,5,7-tetrazocine (HMX). For each of these materials we resolve (at least partially) the underlying THz vibrational spectrum, and present vibrational resonances that have not been reported in previous free space measurements reported in the literature. In waveguide THz-TDS a thin analyte layer is deposited onto the metal surface of a parallel plate waveguide (PPWG) [14,15]. THz waves which are confined within the sub-wavelength (50 micron) gap of the PPWG characterize the vibrational spectrum of the thin layer in a sensitive manner. Recently, we have shown that waveguide THz-TDS has the ability to produce vibrational linewidths in molecular solids that are as narrow as 7 GHz (0.21 cm^{-1}) at cryogenic temperatures [5]. The strong line narrowing reveals many of the underlying vibrational resonances and thereby provides a new opportunity to assign individual lines to specific vibrational motions in the crystalline environment using theoretical models. For 4A-DNT we first present evidence for a structural phase transition as the sample is cooled to near 200 K in the PPWG. With further cooling to 14 K waveguide THz-TDS shows a large number of vibrational lines in the spectral region between 1.0 THz – 4.3 THz. Even so, our measurement suggests there are additional modes that remain unresolved at the current spectral resolution. In the case of PETN our measurement more completely resolves the full underlying vibrational resonances. The PETN spectrum, measured at 12 K, resolves several vibrational lines which had not been observed in previous free space measurements of PETN performed at cryogenic temperatures below 10 K [3,4]. Finally, for HMX, we describe a highly resolved vibrational spectrum which we tentatively assign to the meta-stable gamma polymorph.

2. Experimental

The measurement method for waveguide THz-TDS is outlined in Fig. 1 and uses well established ultrafast optoelectronic techniques to generate and detect sub-picosecond THz pulses [16]. The explosives and simulant materials are cooled to temperatures near 10 K using a two stage He cryocooler.

THz pulses are coupled into and out of a PPWG with a 50 micron gap using plano-cylindrical high resistivity Si lenses at the entrance and exit faces of the assembly. The polarization of the THz field is perpendicular to the waveguide surface. The spectral resolution is 6.7 GHz which corresponds to 150 picosecond scan lengths. Typically, between two and eight temporal scans were averaged to improve the signal to noise ratio. All scans were zero padded by a factor of two to four before performing a Fourier transform to generate the spectral amplitude. Further details regarding the measurement method may be obtained from Reference 5.

To recover the absorbance spectrum, which includes any broadband background absorption, it is necessary to measure the reference spectral amplitude for the empty PPWG. The amplitude absorbance is then obtained as $-\ln(A_{sig}/A_{ref})$, where A_{sig} and A_{ref} are the spectral amplitudes for the PPWG containing the layer and the empty PPWG, respectively. In previous studies we have shown how A_{ref} can be obtained by removing the layer without disturbing the waveguide [17,18]. Here, we use an approximate method to estimate the absorbance spectrum. The reference spectral amplitude is estimated from the film spectral amplitude by choosing points outside the absorption lines and then fitting the points with a smooth function, which includes any broadband absorption. While this method yields only

#135522 - $15.00 USD Received 22 Sep 2010; revised 28 Oct 2010; accepted 2 Nov 2010; published 10 Dec 2010

approximate intensities, and not the broadband absorption, it is possible to extract line frequencies and linewidths.

Thin polycrystalline layers of the explosives and 4A-DNT were formed using simple drop casting from solution. Before preparation of the microcrystalline layer the inner surface of the PPWG was cleansed with solvent and then plasma cleaned. Ampoules containing standard solutions of 4A-DNT, PETN and HMX at 1 milligram/milliliter (acetonitrile) were purchased from Cerilliant, and then concentrated to approximately 2 milligrams/milliliter. Approximately 200 microliters of solution were dropped on the PPWG surface. After evaporation, the relatively thick edges of the film around its perimeter were swabbed away using a solvent soaked swab. This typically produced a film footprint about 10-15 millimeters in width and 10-20 millimeters in length. The morphologies of the microcrystals were characterized under a microscope and recorded as optical micrographs. X-ray diffraction was used as an analytical tool to confirm the integrity and crystallinity of the microcrystals on the waveguide surface, check for polymorphism, and to determine the orientation of the microcrystals on the surface. X-ray diffraction spectra were measured using a Philip's X'pert diffractometer with Cu Kα radiation. The assignment of the peaks in the X-ray diffraction spectrum was made by comparing measured positions to those given in the Cambridge Crystallographic Database using the Mercury 2.3 program.

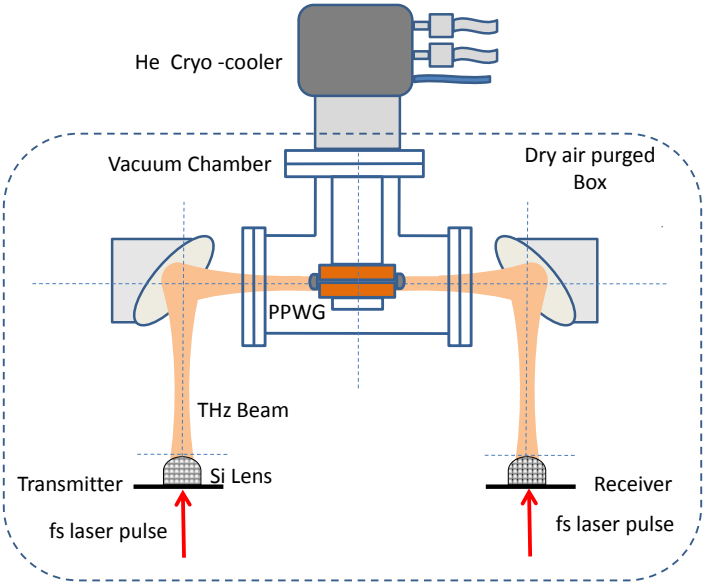

Fig. 1. Schematic of the waveguide THz-TDS apparatus.

3. Results and discussion

The center frequencies and full-width-at-half-maximum (FWHM) linewidths of the observed vibrational lines at the indicated temperatures for 4A-DNT, PETN and HMX are summarized in Table 1.

Table 1. . Line frequencies in THz (and linewidths in GHz) for 4A-DNT, PETN, and HMX.

4A-DNT/Au 14 K	PETN/Au 12 K	HMX/Al 13K
0.744 (12)	1.102 (7)	0.905 (13)
0.882	1.707 (11)	1.220 (18)
0.901	2.14	1.420 (18)

#135522 - $15.00 USD Received 22 Sep 2010; revised 28 Oct 2010; accepted 2 Nov 2010; published 10 Dec 2010

0.917	2.241 (39)	1.541 (34)
1.052 (11)	2.348 (33)	1.656 (44)
1.497 (23)	2.556 (19)	1.772 (51)
1.871	2.938 (31)	2.063
1.924	3.07 (41)	2.10 (sh)
2.206 (16)	3.226 (35)	2.29
2.270 (28)	3.351	2.44
2.475	3.42	2.78
2.557		3.10
2.97		3.16 (sh)
3.03		
3.23		
3.35		

3.1 4-amino-dinitrotoluene

The molecule 4A-DNT is a product formed by the chemical reduction of the explosive trinitrotoluene (TNT) [19]. For example, in TNT contaminated soils the reduction of TNT via bacterial enzymes produces 4A-DNT as an intermediate compound to the fully reduced 2,4,6-triaminotoluene. X-ray diffraction measurements have shown two crystalline forms for 4A-DNT. At room temperature 4A-DNT crystallizes in the orthorhombic unit cell, $Cmc2_1$, with 4 molecules per unit cell (Z = 4) [19]. X-ray diffraction measurements at 150 K show that 4A-DNT crystallizes in a triclinic unit cell with Z = 4 [20].

4A-DNT was drop cast onto an Au-coated waveguide plate with an estimated mass of ~200 μg. The optical micrograph in Fig. 2 shows a polycrystalline needle-like morphology with planar ordering with respect to the surface. The X-ray diffraction measurement at room temperature in Fig. 2 shows only three lines, at diffraction angles consistent with the $Cmc2_1$ unit cell of 4A-DNT. The X-ray diffraction pattern in Fig. 2 suggests that the 4A-DNT layer is highly oriented with the (110) plane parallel to the PPWG surface. We note that the width of the diffraction lines is about 0.08 degrees and essentially instrument limited. The sharpness of the diffraction lines is indicative of high crystallinity.

The THz temporal waveforms were collected at room temperature, 90 K, and 14 K. The scans at 90 K and 14 K were collected over a 150 picosecond time window, which was sufficient for the THz transient signal to decay into the noise floor. The corresponding spectral amplitudes are shown in Fig. 3. At room temperature the spectral amplitude shows two absorption features near 1.26 THz and 1.6 THz, and a broad feature near 2.6 THz. These signatures are consistent with a previous pellet measurement of 4A-DNT [8]. Several new absorption features begin to appear as the PPWG is cooled to 90 K. Most noticeable is the relatively intense absorption near 1.5 THz. Finally, at 14 K strong line narrowing is observed and the spectral amplitude reveals a substantial increase in information about the underlying vibrational modes of 4A-DNT.

In Fig. 3 we note the large fractional blue shift (~20%) of the absorption line near 1.26 THz (293 K) and the disappearance of the line near 1.58 THz (293 K) when the PPWG is cooled to 90 K. This observation suggests a structural phase transition between room temperature and 90 K. To further examine this possibility, we measured a more detailed temperature dependence of the THz signal waveform as the temperature was lowered in increments of ≤ 10 K from room temperature to 90 K. We also measured temperature dependent waveforms as 4A-DNT was warmed back to room temperature. The results are summarized as spectral amplitudes in Figs. 4a and 4b. Figure 4a shows the spectral amplitudes as 4A-DNT is cooled over a narrow temperature range where an abrupt change occurs in the absorption features. At 180 K the spectral amplitude shows essentially the same two absorption features observed at room temperature (Fig. 3), except a small blue shift in the

#135522 - $15.00 USD Received 22 Sep 2010; revised 28 Oct 2010; accepted 2 Nov 2010; published 10 Dec 2010

line frequencies due to the lower temperature. At 178 K an abrupt change occurs, where a new feature appears at 1.38 THz, which is accompanied by both the attenuation of the feature at

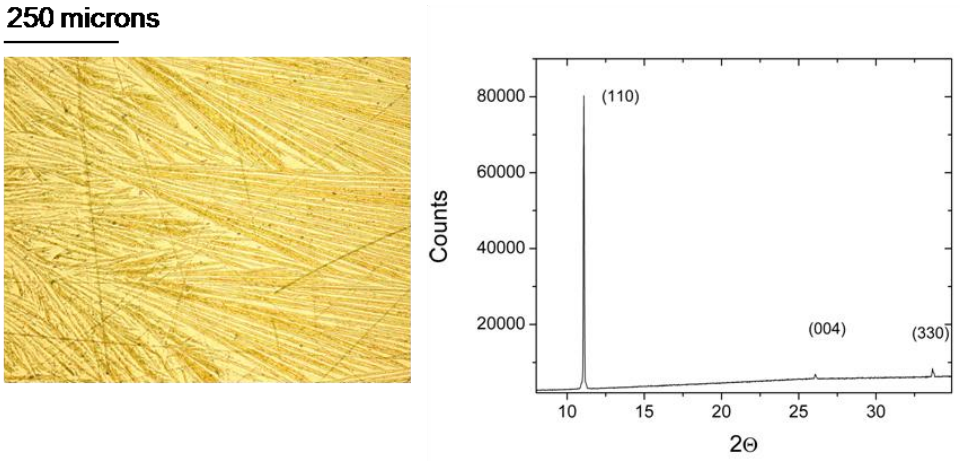

Fig. 2. Left: Optical micrograph of 4A-DNT on Au at 20 X magnification. Right: X-ray diffraction spectrum of the 4A-DNT layer on Au. Assignments to crystal planes are shown in parenthesis.

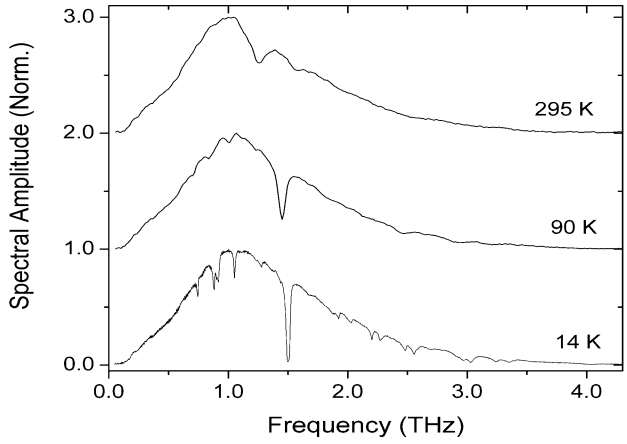

Fig. 3. Normalized spectral amplitudes of 4A-DNT on Au for three temperatures.

1.26 THz, and the disappearance of the feature at 1.58 THz. At 176 K the spectrum consists mostly of the feature 1.38 THz. Figure 4b shows the evolution of spectral amplitudes as 4A-DNT is warmed. In this case the changes in mode frequencies occur at a higher temperature near 200 K. At 190 K the spectral amplitude shows only the feature at 1.38 THz; at 200 K all three features appear; at 210 K only the features at 1.26 THz and 1.58 THz appear. Based on the X-ray diffraction measurements in the literature showing a triclinic structure at 150 K [19], and our room temperature X-ray diffraction of 4A-DNT on Au showing an orthorhombic structure, we conclude that the abrupt changes in the THz absorption features indicate a conversion between orthorhombic and triclinic structures. The orthorhombic to triclinic transition occurs over a relatively sharp range of 4 degrees during cooling near 178 K. Upon warming a hysteresis of about 20 K is observed where the triclinic to orthorhombic transition occurs near 200 K, and over a wider temperature range of about 20 K.

#135522 - $15.00 USD Received 22 Sep 2010; revised 28 Oct 2010; accepted 2 Nov 2010; published 10 Dec 2010

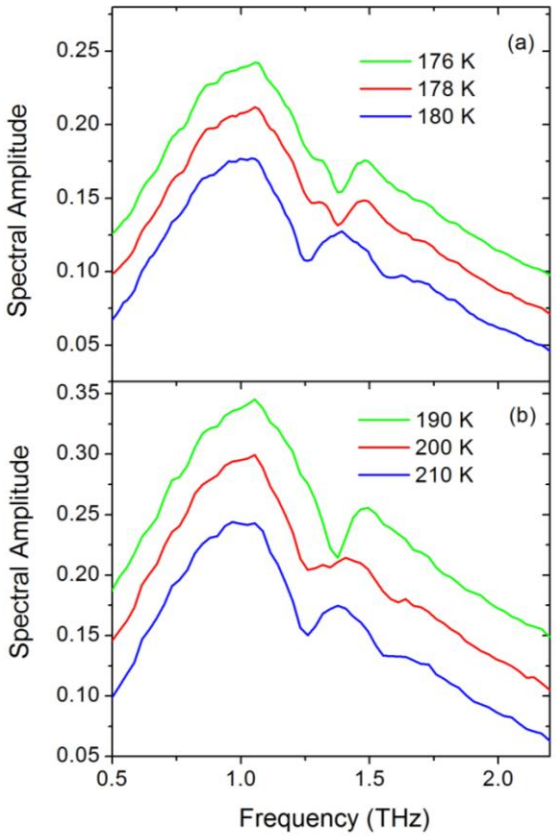

Fig. 4. Spectral amplitudes for 4A-DNT measured where the THz line structure changes abruptly with temperature. (a): Spectral changes upon cooling near 178 K. (b): Spectral changes upon warming near 200 K. In both (a) and (b) the spectral amplitudes are offset for clarity.

Figure 5 shows the amplitude absorbance spectrum of 4A-DNT measured at 14 K, which consists of a complex pattern of vibrational lines, some of which are only partially resolved. For example, the series of lines in the inset of Fig. 5 suggests at least five lines are present, where the middle feature near 0.9 THz suggests at least three lines. In the region between 0.5 THz and 4.3 THz we estimate that the spectrum contains at least 16 lines. In previous works, we have demonstrated the ability of waveguide THz-TDS to measure line frequencies with a precision approaching 1 GHz [18]. We find similar precision here over the central part (0.7 – 1.5 THz) of the spectrum where the signal to noise ratio is the highest. The narrowest line occurs at 1.051THz with a FWHM linewidth of 11 GHz. The strong feature at 1.497 THz has a FWHM linewidth of 23 GHz. Figures 6a and 6b shows these two lines on an expanded frequency scale. The narrow line at 1.051 THz (Fig. 6a) is sufficiently isolated to allow simple lineshape analysis and we have used a non-linear least squares fit to the experimental spectrum using either a single Lorentzian or Gaussian function. For this line the Lorentzian lineshape (FWHM = 10.5 GHz) clearly represents a better approximation to the experimental lineshape. The strong absorption at 1.497 THz (Fig. 6b) has a more complex lineshape. There is evidence for two weak shoulder features on the high frequency side of the lineshape which suggests that the line is a superposition of closely spaced resonances. The complexity of the 4A-DNT spectrum is partly related to the triclinic unit cell containing four molecules. In this case 21 optical phonons are predicted, many of which will fall within the spectral bandwidth of the measurement.

#135522 - $15.00 USD Received 22 Sep 2010; revised 28 Oct 2010; accepted 2 Nov 2010; published 10 Dec 2010

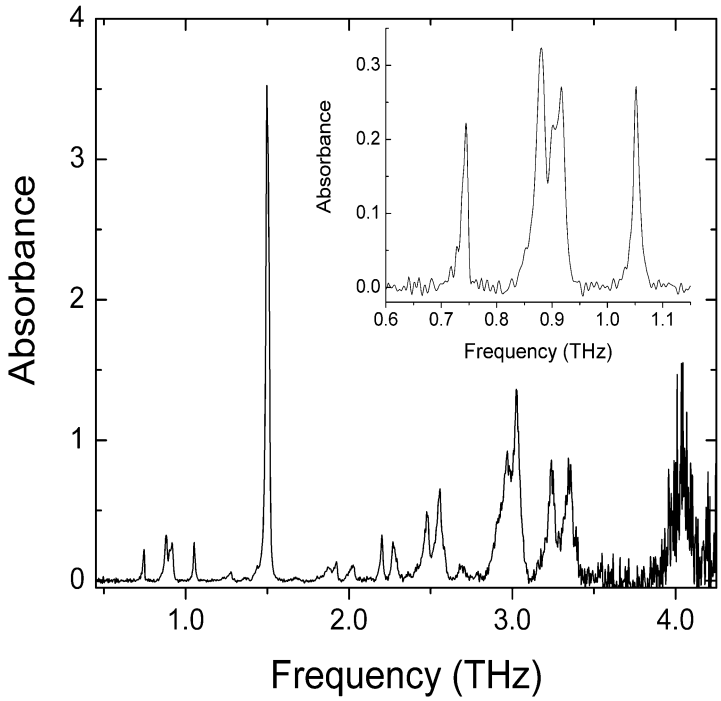

Fig. 5. Amplitude absorbance spectrum for 4A-DNT on Au at 14 K. The inset shows the lower frequency part of the spectrum on an expanded scale.

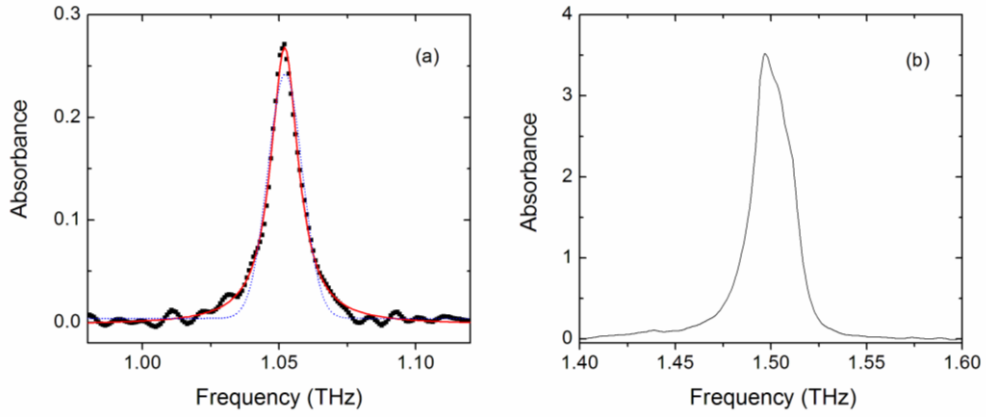

Fig. 6. (a): Lineshape of the 1.051 THz mode (dots) with non-linear least square fits using a Lorenztian function (red line) or a Gaussian function (blue line). (b): Experimental lineshape of the strong feature at 1.497 THz.

3.2 PETN

The most stable form of the explosive PETN crystallizes in the orthorhombic space group P-42_1c with Z = 2 [21]. In this case nine phonon modes are predicted, thus a simpler THz vibrational spectrum is anticipated for PETN compared to 4A-DNT. In the range between 0.2 THz and 3.0 THz there have been several free space THz spectroscopy measurements made for PETN in a mixed pellet form [3,7,8,10], and a THz measurement for a PETN single

#135522 - $15.00 USD Received 22 Sep 2010; revised 28 Oct 2010; accepted 2 Nov 2010; published 10 Dec 2010

crystal [4]. At room temperature, the PETN pellet shows two prominent absorption lines near 2.0 THz and 2.8 THz with FWHM linewidths greater than 200 GHz.

A PETN layer was formed on an Au-coated PPWG surface by drop casting from a 2 mg/ml solution in acetonitrile. The estimated mass is 150 μg. PETN on Au forms a dendritic type of morphology as shown in the optical micrograph of Fig. 7. An *equivalent homogeneous layer thickness* of approximately 400 nanometers is estimated by using the density of PETN (1.77 g/cm3), and considering that the estimated mass of 150 μg is spread over an area of approximately 2 cm^2. X-ray diffraction (Fig. 7) confirmed the integrity of the PETN microcrystals. The appearance of several diffraction lines could be assigned to crystalline planes of PETN and indicates that the microcrystals are not highly oriented.

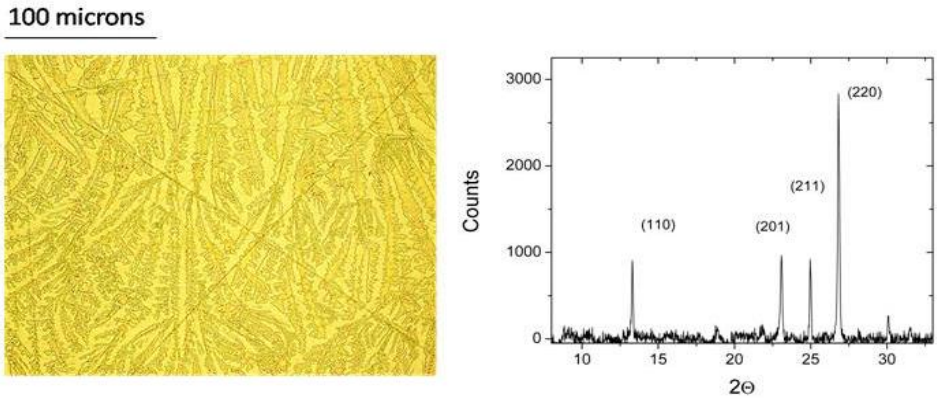

Fig. 7. Left: Optical micrograph of PETN on Au at 50 X magnification. Right: X-ray diffraction spectrum of PETN on Au. Assignment to crystal planes is given in parenthesis.

Figures 8a and 8b show the amplitude absorbance spectrum of PETN on Au measured at room temperature and 12 K, respectively. The room temperature spectrum shows three absorption features at 2.01 THz, 2.04 THz and 2.92 THz. These frequencies are in reasonable agreement with recent free space measurements of PETN pellet samples at room temperature [8]. One notable difference in our measurement is that the feature near 2 THz shows a somewhat smaller relative intensity with respect to the 2.92 THz feature. This may be due to a partial orientation of the microcrystals.

The 12 K measurement in Fig. 8b shows a highly resolved underlying THz vibrational spectrum consisting of a series of eleven lines between 1.0 THz and 3.5 THz. The sharp lines of the PETN layer can be correlated with the relatively broad absorption features of our room temperature measurement, and also with those of the previous free space THz measurements of PETN pellets [3] (both at room temperature and 4 K). For example, the broad absorption feature near 2.0 THz undergoes a blue shift of 0.21 THz (7.0 cm^{-1}) upon cooling to 12 K, and splits into four lines that include the relatively strong doublet of lines at 2.234 THz and 2.349 THz, and the weaker lines at 2.14 THz and 2.555 THz. In addition, the broad absorption feature of the PETN pellet near 2.8 THz splits into five lines for the PETN layer at 12 K. The prominent line near 2.24 THz has a FWHM linewidth of about 30 GHz in the 12 K spectrum. This represents about a factor of about 7 in line narrowing when compared to ~200 GHz linewidth of the room temperature line at 2.01 THz. The high sensitivity and high spectral resolution of the measurement are highlighted by the observation of weak lines at 1.101 THz and 1.710 THz. These lines have FWHM linewidths of 7 GHz and 10 GHz, respectively. We have observed these weak lines in waveguide THz-TDS measurements of other PETN layers on waveguide surfaces.

#135522 - $15.00 USD Received 22 Sep 2010; revised 28 Oct 2010; accepted 2 Nov 2010; published 10 Dec 2010

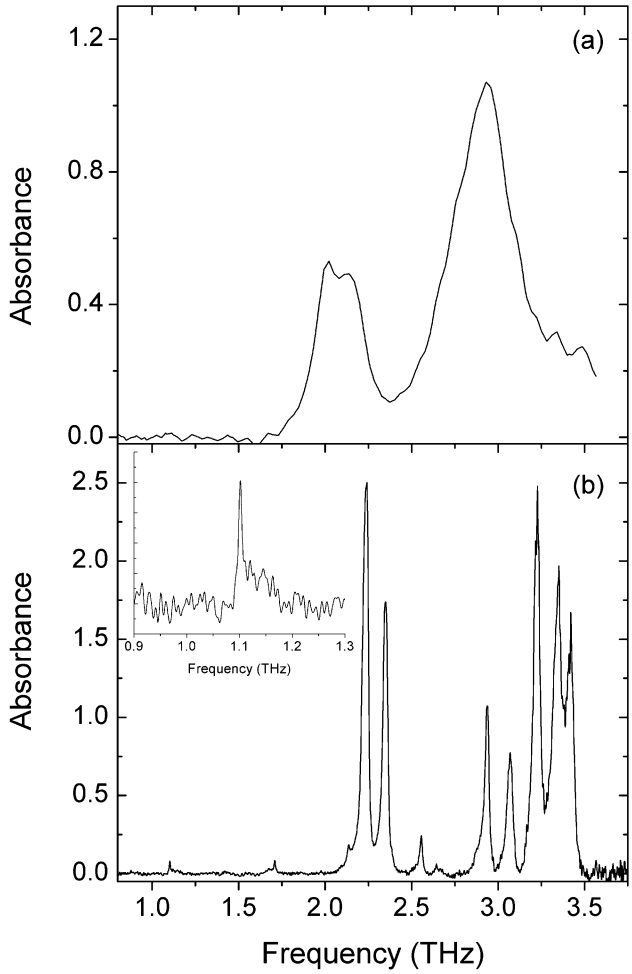

Fig. 8. (a) Absorbance spectrum of PETN on Au at room temperature. (b) Absorbance spectrum of PETN on Au at 12 K. Inset: The lowest frequency mode of PETN on an expanded scale.

We compare the waveguide THz-TDS measurement of the PETN layer to previous free space THz measurements of PETN in pressed pellet form (mixed with a transparent polymer) at 4 K [3], and a single crystal measured at 8 K [4]. For the PETN pellet cooling to 4 K resulted in strong blue shifting of the absorption features, though only partial resolution of the individual THz resonances occurred [3]. For the PETN pellet the prominent absorption feature near 2 THz showed a FWHM linewidth of about 300 GHz [3]. This may be compared to the quartet of lines in Fig. 8b for our waveguide THz-TDS measurement, with FWHM linewidths ranging between 20 GHz – 40 GHz. For the absorption feature near 2.8 THz, the cryogenic pellet spectrum showed several shoulder features which suggested a rich underlying THz spectrum [3]. A stronger line narrowing was observed for the PETN single crystal measured at 8 K and using two different crystal orientations [4]. This measurement covered the spectral range up to about 2.4 THz (80 cm^{-1}) and resolved many of the features observed in our measurement. The FWHM linewidths from the measurement of the PETN crystal appear to be between 100 GHz - 150 GHz [4], which is broader than the corresponding lines measured for the PETN microcrystals on Au (see Table 1).

#135522 - $15.00 USD Received 22 Sep 2010; revised 28 Oct 2010; accepted 2 Nov 2010; published 10 Dec 2010

4.3 HMX

The β polymorph is the most stable form of the four polymorphs (α,β,γ,δ) of HMX and the room temperature THz spectrum of β-HMX has been measured by several groups [7,8,10]. Recent work has measured the room temperature THz spectrum of the α-polymorph, as well as the γ-polymorph, which is a hydrated form of HMX [22]. This work showed the strong dependence of the THz spectrum on the crystalline form of HMX [22]. In our work we anticipated making the β-form of HMX using the drop casting method. In the first attempt HMX microcrystals were formed on an Al PPWG surface under ambient conditions by drop casting from the standard solution in acetonitrile. The optical micrograph in Fig. 9 (left) shows that individual microcrystals formed with a planar ordering with respect to the surface. However, the X-ray diffraction spectrum shown in Fig. 9 (right) is consistent with the γ-HMX polymorph and with microcrystals highly oriented with the (200) plane parallel to the Al surface. We did not observe any diffraction lines that could be correlated with β-HMX. Several additional attempts were made on copper and gold surfaces, both in the ambient environment and in a dry N_2 environment; however in each case the X-ray diffraction spectrum indicated only the presence of γ-HMX. It's possible that there was sufficient water retained in the acetonitrile solvent, or enough residual water adsorbed on the metal surface, to induce the formation of γ-HMX after drop casting. We note that γ-HMX has been described as metastable at all temperatures and pressures and is usually formed under conditions of rapid crystallization [23].

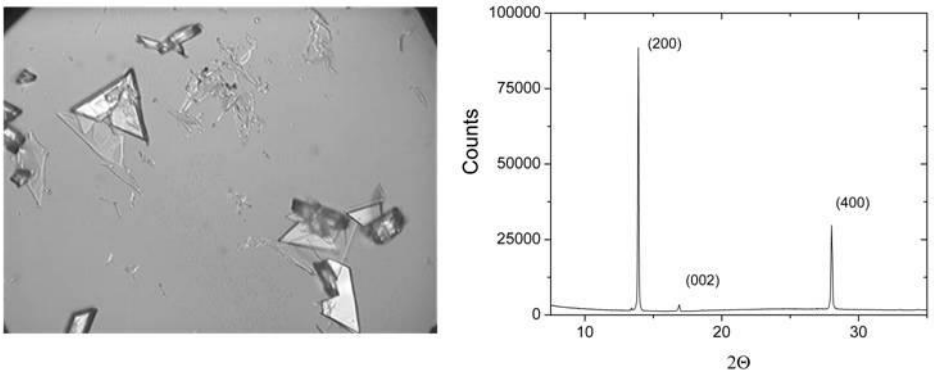

Fig. 9. Left: Optical micrograph of HMX on A1 at 40 X magnification. Right: X-ray diffraction spectrum of HMX on A1. Assignment to crystal planes is given in parenthesis.

The spectral amplitudes for the HMX layer on Al as a function of temperature are shown in Fig. 10. At room temperature we observe an absorption feature near 1.5 THz and a second broader feature near 2.5 THz. Upon cooling these features sharpen and undergo a monotonic blue shift. At 80 K several relatively sharp features appear below 1.5 THz and also above 2.0 THz. Upon further cooling to 13 K these lines continue to sharpen, but undergo only small additional blue shifts.

Figure 11a shows the absorbance spectrum for HMX on A1 at 13 K. Clearly, the broad absorption feature at room temperature has split into two lines. In addition, the line narrowing at 13 K has revealed as many 11 lines between 0.9 THz and 3.2 THz. For comparison, Fig. 11b shows a second HMX layer cast on a Cu PPWG and characterized at 12 K. While the signal to noise is not as high for this sample, all of the major lines are reproduced with similar relative intensities.

The gradual evolution of spectral amplitudes with cooling (Fig. 10) does not show the "abrupt" changes that would indicate a significant conversion to another polymorph. Thus, we suggest that the temperature dependent spectra of Figs. 10 and 11 are due primarily to γ-HMX. If some interconversion occurs during cooling then β-HMX is the most likely

#135522 - $15.00 USD Received 22 Sep 2010; revised 28 Oct 2010; accepted 2 Nov 2010; published 10 Dec 2010

polymorph to be formed. The α-HMX and δ-HMX forms are described as stable above room temperature: α-HMX is stable from 377 K to 429 K [24], and δ-HMX is stable above 429 K [25]. While these polymorphs can exist at room temperature for days, they are initially prepared at elevated temperatures by heating β-HMX crystals in solution. Thus, it seems unlikely that cooling the γ-HMX microcrystals would produce the α or δ polymorphs. The presence of γ-HMX at low temperatures is also supported by the significant mode structure at frequencies below 1.8 THz. For example, if a significant conversion from γ-HMX to β-HMX occurred then these modes would tend to disappear because β-HMX does not show vibrational modes below about 1.75 THz [7,8,26]. We cannot totally rule out a partial interconversion to β-HMX. This would be identified in the THz spectrum at low temperature by specific line frequencies above 1.8 THz.

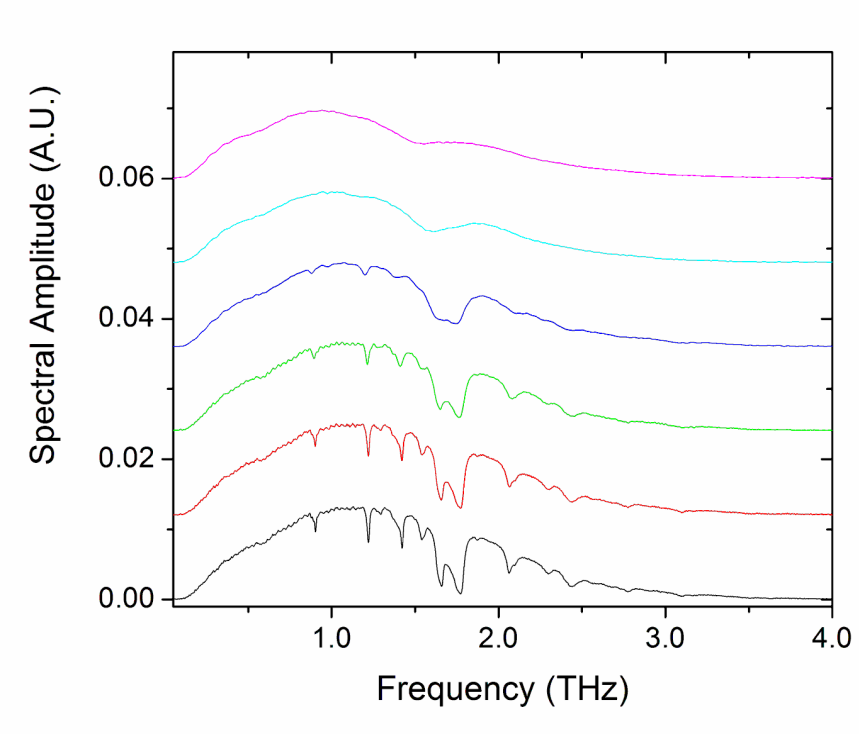

Fig. 10. Temperature dependence of the spectral amplitudes for HMX on Al . Room temperature (magenta), 190 K (cyan), 80 K (blue), 40 K (green), 20 K (red), 13 K (black).

5. Conclusions

We have measured the temperature dependent THz vibrational spectra for the explosives related solids 4A-DNT, PETN and HMX using waveguide THz-TDS. Each of these materials formed a thin polycrystalline layer on the surface of a PPWG and exhibited a strong line narrowing effect as the sample was cooled to cryogenic temperature. For these materials we have shown that the simple method of drop casting from solution provides a micro-crystalline layer of sufficient crystallinity to achieve highly resolved THz spectra at cryogenic temperatures and with FWHM linewidths as narrow as 7 GHz. For the case of 4A-DNT we presented evidence for a structural phase transition near 200 K. Based on the known polymorphs for 4A-DNT, we propose that there is a conversion from orthorhombic to triclinic structures as 4A-DNT is cooled through the transition point. At low temperature, 4A-DNT revealed a complex underlying spectrum that is consistent with a unit cell containing four molecules. Our waveguide THz-TDS measurement for PETN revealed several new vibrational lines that had not been observed in previous free space THz measurements of a

#135522 - $15.00 USD Received 22 Sep 2010; revised 28 Oct 2010; accepted 2 Nov 2010; published 10 Dec 2010

pellet and a single crystal samples at cryogenic temperature. We note that the easy-to-prepare polycrystalline PETN layer produced linewidths that were at least as narrow as observed for a single crystal measurement at similar cryogenic temperature. Finally, for the case of an HMX layer at 13 K, we described a highly resolved THz spectrum which we have tentatively assigned to the γ-polymorph. We suggest that narrow-line waveguide THz-TDS measurements, such as described here, can be used to test computational models for predicting THz spectra [27], and help to advance fundamental understandings of THz vibrational fingerprint spectra.

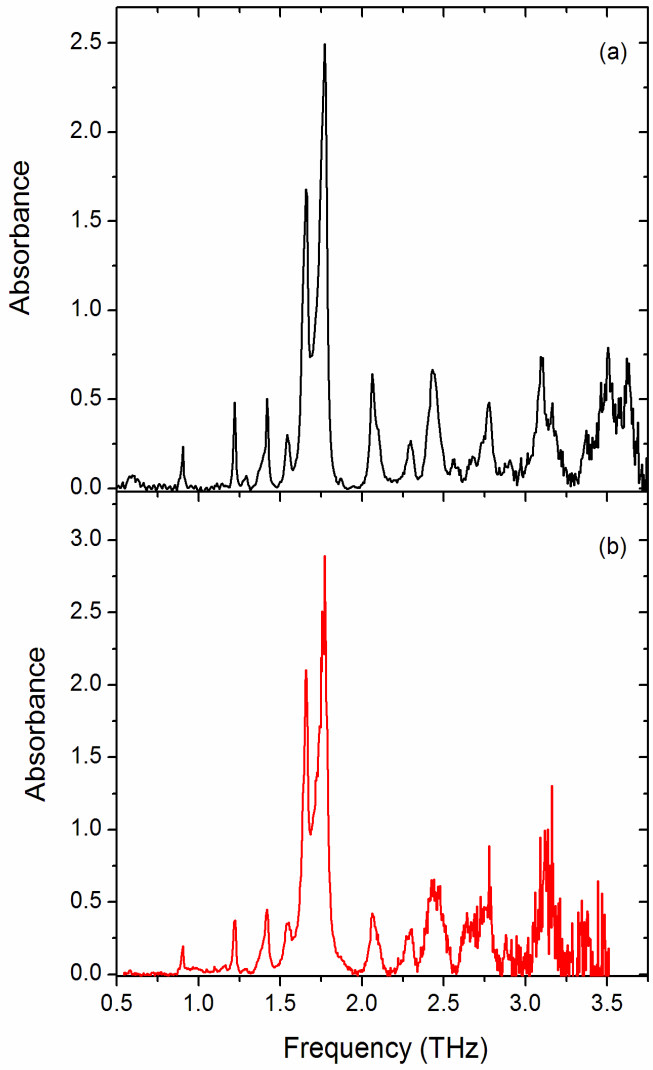

Fig. 11. Absorbance spectra for two different samples of HMX at cryogenic temperature. (a) HMX on Al at 13 K. (b) HMX on Cu at 12 K.

Acknowledgements

This work was supported by the Office of Naval Research and the Defense Threat Reduction Agency (10-2960M).

#135522 - $15.00 USD Received 22 Sep 2010; revised 28 Oct 2010; accepted 2 Nov 2010; published 10 Dec 2010